

A SUBMILLIMETER SURVEY OF GRAVITATIONALLY LENSED QUASARS

RICHARD BARVAINIS

National Science Foundation, Arlington, VA 22230
4201 Wilson Boulevard, Arlington, VA 22230 USA
rbarvai@nsf.gov

AND

ROB IVISON

Royal Observatory, Edinburgh
Blackford Hill, Edinburgh, EH9 3HJ UK
rji@roe.ac.uk

Accepted for publication in the Astrophysical Journal

ABSTRACT

Submillimeter (and in some cases millimeter) wavelength continuum measurements are presented for a sample of 40 active galactic nuclei (probably all quasars) lensed by foreground galaxies. The object of this study is to use the lensing boost, anywhere from $\sim 3 - 20$ times, to detect dust emission from more typical AGNs than the extremely luminous ones currently accessible without lensing. The sources are a mix of radio loud and radio quiet quasars, and, after correction for synchrotron radiation (in the few cases where necessary), 23 of the 40 (58%) are detected in dust emission at $850\mu\text{m}$; 11 are also detected at $450\mu\text{m}$. Dust luminosities and masses are derived after correction for lensing magnification, and luminosities are plotted against redshift from $z = 1$ to $z = 4.4$, the redshift range of the sample. The main conclusions are (1) Monochromatic submillimeter luminosities of quasars are, on average, only a few times greater than those of local IRAS galaxies; (2) Radio quiet and radio loud quasars do not differ significantly in their dust luminosity; (3) Mean dust luminosities of quasars and radio galaxies over the same redshift range are comparable; (4) Quasars and radio galaxies alike show evidence for more luminous and massive dust sources toward higher redshift, consistent with an early epoch of formation and possibly indicating that the percentage of obscured AGNs increases with redshift.

Subject headings: gravitational lensing—quasars:general—submillimeter

1. INTRODUCTION

Strong dust emission at infrared and submillimeter wavelengths is now recognized as a fundamental tracer of activity in galaxies, be it star formation or processes related to nuclear black holes. Ordinary, quiescent galaxies like the Milky Way exhibit dust luminosities of order $10^{10} L_{\odot}$, but active systems, such as ultraluminous infrared galaxies (ULIRGs), quasars, and radio galaxies can be as much as 10^3 times more powerful (Sanders & Mirabel 1996). In these objects the intense dust emission appears to be triggered by galaxy interactions and mergers, which are thought to be responsible at least in part for the formation and growth of massive elliptical galaxies and the supermassive black holes found in their nuclei (e.g., Kormendy & Sanders 1992; van Dokkum et al. 1999).

In the mid-1980s the IRAS mission discovered many infrared-luminous galaxies and quasars at low redshifts in the mid- to far-infrared ($12-100\mu\text{m}$), establishing dust emission as an important if not dominant component of the bolometric luminosity in certain classes of objects. The dust luminosity is a result of reprocessing of shorter wavelength optical/UV radiation originating either from hot young stars, in the case of starbursts, or from the release of gravitational energy as material accretes onto a nuclear black hole, in the case of quasars. In some galaxies both starburst and quasar activity are likely to contribute, and there remains some dispute over which process dominates

in various types of objects.

Although the findings of IRAS were revolutionary for the local universe, its sensitivity was such that only a few high-redshift systems were detected: the quasar PG 1634+607 ($z = 1.3$), the ULIRG/buried quasar IRAS F10214+4724 ($z = 2.3$), the Cloverleaf quasar (H 1413+117; $z = 2.6$), and the $z = 3.9$ broad absorption line quasar APM 08279+5255 (Rowan-Robinson et al. 1991; Barvainis et al. 1995; Lewis et al. 1998). The latter three are strongly magnified by gravitational lensing, boosting their fluxes above the IRAS detection thresholds at 60 and $100\mu\text{m}$. Further progress was made at submillimeter wavelengths at the James Clerk Maxwell Telescope (JCMT), first using the single-channel photometer UKT14, then later with the submillimeter camera SCUBA. F10214+4724 and the Cloverleaf were detected at 800 and $450\mu\text{m}$ (Rowan-Robinson et al. 1993; Barvainis et al. 1992), to be followed by several other quasars and radio galaxies (Hughes et al. 1997). To date the census of published submillimeter detections of high redshift objects numbers ~ 150 (mostly unidentified), some of which are either strongly lensed by individual galaxies or weakly lensed by galaxy clusters (Smail, Ivison, & Blain 1997).

The high sensitivity of SCUBA, combined with the flux boost provided by strong lensing, presents an opportunity to delve deeper into the submillimeter luminosity function than would otherwise be possible. The majority of unlensed quasars are undetectable with current

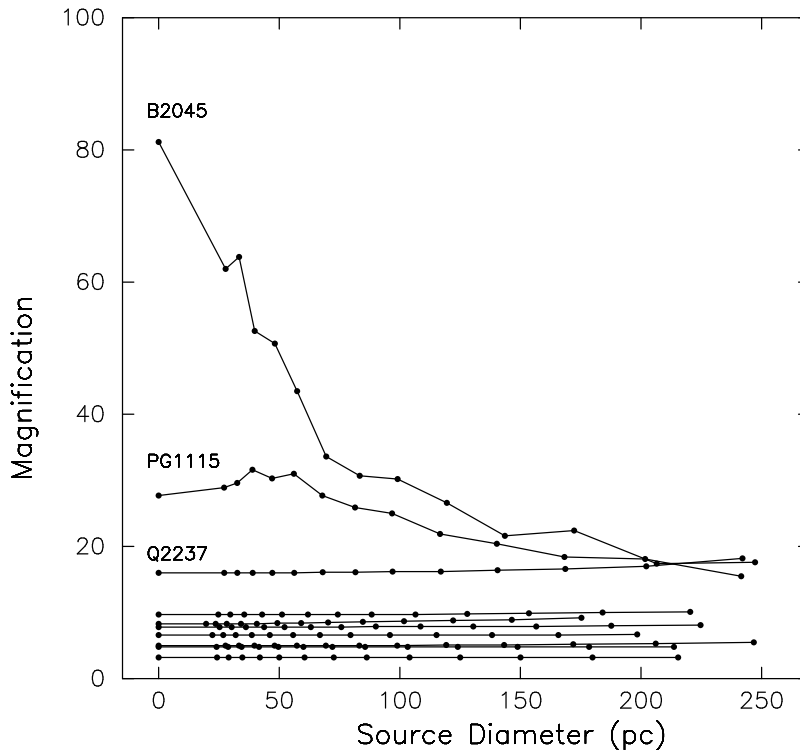


FIG. 1.— Modeled magnification versus source diameter for some of the lensed quasars in the sample. The model for the intervening lens, based on optical data, is applied to successively larger sources at the quasar to determine the net magnification. Magnifications that are high for the optical emission (essentially a point source) tend to drop to about 20 as the source size increases to ~ 200 pc (a likely minimum dust source size). At low magnifications the magnification tends to be constant with source size (unlabelled examples plotted include SBS 0909+532, BRI 0951+2635, LBQS 1009–0252, HST 12531–2914, HST 14113+5211, H 1413+117, and HST 14176+5226). Model results generated by B. McLeod (private communication).

instruments, so up to now *typical* dust luminosities and masses of active galaxies at high redshift have remained unknown. Only the very highest luminosities can be detected without lensing. However, there are now about 50 known strongly lensed objects, most of which are in fact quasars (see the CASTLeS compilation, <http://cfa-www.harvard.edu/castles>). This paper reports the results of a submillimeter survey of a large fraction of the known lensed quasars, presenting data on a sample of 40 objects in which dust emission has been clearly detected at $850\mu\text{m}$ and/or $450\mu\text{m}$, or meaningfully constrained by upper limits.

These lensed quasars, while not a complete sample by any definitive criteria, are nevertheless a random, passively selected sample of quasars at high redshift – they are quasars that happen to lie behind massive galaxies. With a typical lensing boost of an order of magnitude, they provide a unique window on the dust content of active galaxies in the early universe.

2. OBSERVATIONS AND RESULTS

2.1. Data

Of the submillimeter results on 40 lensed quasars listed in Table 1, 39 are from our own observations and one (F10214+4724) is from Rowan-Robinson et al. (1993). APM 0879+5255 was originally detected by Lewis et al. (1998), but our own higher SNR observations are used here. Table 1 also reports 3mm and 1.3mm fluxes for a number of sources. In radio loud objects these longer wavelength data are useful for correcting synchrotron con-

tamination of the submillimeter fluxes to derive an estimate of the true dust emission level.

The submillimeter observations were made over a series of observing runs at the JCMT during 1999–2001. The submillimeter camera SCUBA (Holland et al. 1999) was used in photometry mode, observing simultaneously at $450\mu\text{m}$ and $850\mu\text{m}$, with the target centered on the central bolometer of SCUBA’s back-to-back arrays. The JCMT’s secondary mirror was chopped azimuthally by $60''$ at 7 Hz while jiggling through a 9-point filled-square pattern, the points separated by $2''$. The telescope was nodded in azimuth by $60''$ following the completion of each jiggle pattern, in an object-sky-sky-object pattern designed to keep the source constantly in one of the chop beams. Atmospheric opacity, pointing accuracy, and focus position were checked every 30 – 60 min and calibration scans of Uranus or Mars were obtained each night. Data were analysed using SURF (Jenness & Lightfoot 1998) following the standard recipes (Stevens, Ivison, & Jenness 1997).

RMS errors for the SCUBA data range from 0.9 to 3.6 mJy (1σ) at $850\mu\text{m}$, depending on time spent on source and weather conditions. At $450\mu\text{m}$ atmospheric transmission is much poorer than at $850\mu\text{m}$, and meaningful fluxes or upper limits at this wavelength were obtained only during the best conditions.

All 3mm continuum fluxes are from the IRAM Plateau de Bure Interferometer (PdBI), and all but one were obtained by us during a search for CO emission from lensed quasars (Barvainis, Alloin, & Bremer 2002; the 3mm flux for 0957+561 is from Planesas et al. 1999). The 1.3mm

data were obtained either with the IRAM 30m telescope bolometer, with the PdBI, or with the 1.3mm channel on SCUBA (see notes to Table 1).

Upper limits given in Table 1 are 2.5 times the 1σ statistical uncertainties. Quoted errors do not include absolute calibration uncertainties, estimated to be in the range 5 – 10%.

2.2. Lensing Magnifications

In order to calculate source luminosities, lensing must be taken into account. Estimates of the lensing magnifications were obtained for 30 of the 40 sources, either from the literature or via private communication. These magnifications are generally derived from either optical or radio images, and refer to a very compact source of emission. When such a source is very close to a lensing caustic, the magnification can be quite high – over 100 in extreme cases. In the optical, emission is from the primary quasar optical/UV source which has a size scale of order 10^{-3} pc. Boosting derived from radio images often refers to a flat-spectrum core, also on scales of well under a parsec.

The basic problem in estimating the magnifications of the dust sources is that the size scales for submillimeter dust emission are tens to hundreds of parsecs rather than subparsec, and sources on these scales will tend to have lower overall magnifications, particularly when the optically-derived magnifications are high (i.e., when the optical source is very close to a caustic). A large source will have only a small fraction of its area near enough to a caustic to be highly magnified, with other portions farther away and therefore magnified less. This “chromatic” lensing effect, sometimes called differential magnification, has been discussed by Blain (1999). The magnification of a point source is expected to fall approximately linearly with separation from a caustic line in the source plane.

Short of modelling the dust sources themselves, which is not possible since images of the dust are not available, this problem can be dealt with only approximately at best. Weak magnifications in the optical mean that the quasar nucleus is relatively far from a caustic, in which case the dust source will most likely get a comparable overall boost to that of the optical. At high optical magnifications, the boost for the dust source will be lower. Brian McLeod has provided us with model magnifications for some of the quasars in this sample. His results show that magnification decreases with source size for high optical magnifications, and flattens out at about $m = 20$ for sources $\gtrsim 200$ pc. This is likely to be a minimum submillimeter/molecular source size (see Downes et al. 1995; Downes et al. 1999; Kneib et al. 1997). However, at magnifications $\lesssim 20$ the boost is essentially independent of source size. This is illustrated in Figure 1.

Based on this rough guidance, dust magnifications are set as follows: for weak to moderate values, in the range 2.5 – 20, the optical or radio core magnifications are used (see Table 2); for magnifications greater than 20, 20 is adopted as the value; for sources with no available lensing model, m is set to 10. This procedure, while inexact, will generally provide $850\mu\text{m}$ magnifications accurate to within a factor of two or so for most sources, and should not be biased.

2.3. Redshifts

Of the 40 sources in the sample, 33 have measured redshifts. All of these objects have broad emission lines and are therefore classified as quasars. Of the remaining 7 without detected emission lines, one is radio quiet and likely to be a quasar, and 6 are radio loud and could be either quasars or radio galaxies. The mean of the measured redshifts is 2.4, so for purposes of statistical analysis of the luminosities the unmeasured redshifts are set to this value, as indicated in Table 2. Derived dust luminosities and masses (see below) are only weakly dependent on z because of the strong negative K-correction that applies to submillimeter dust emission, so adopting an intermediate redshift for the seven sources without redshifts should not greatly affect the statistical results.

2.4. Corrected Fluxes, Luminosities, and Dust Masses

Table 2 gives assumed magnifications and redshifts, corrected $850\mu\text{m}$ fluxes (as described below), and calculated $850\mu\text{m}$ dust luminosities and dust masses. Luminosities and masses are provided for $H_0 = 50 \text{ km s}^{-1} \text{ Mpc}^{-1}$, and two values of the cosmological density parameter, $\Omega_0 = 1.0$ and 0.1. These parameter values were chosen to facilitate direct comparison with the recent $850\mu\text{m}$ study of high redshift radio galaxies by Archibald et al. (2001; hereinafter ADH01). For simplicity it is assumed that $\Omega_0 = \Omega_M$, the mass density parameter, and $\Omega_\Lambda = 0$; luminosity calculations with the popular $\Omega_M = 0.3$ and $\Omega_\Lambda = 0.7$ cosmology would lie close to the $\Omega_0 = 0.1$ case for low redshifts, and roughly in the middle between $\Omega_0 = 0.1$ and 1.0 at high redshift.

For some of the radio loud objects the centimeter wavelength synchrotron emission, extended to short wavelengths, can contaminate the submillimeter fluxes. In most cases sufficient data are available at 3mm and 1.3mm to fit a synchrotron plus dust emission model. A power law is assumed for the synchrotron, and an optically thin isothermal dust emission template with $T_{\text{dust}} = 40\text{K}$ and emissivity index $\eta = 1.5$. The fitted function is

$$S_\nu = a\nu_r^\alpha + b\nu_r^{4.5}/[\exp(h\nu_r/kT_{\text{dust}}) - 1], \quad (1)$$

where $\nu_r = (1+z)\nu$ is the frequency in the quasar rest frame. This allows separation of the dust and synchrotron components and calculation of the uncontaminated $850\mu\text{m}$ flux. The fit indicates all synchrotron and no dust for B0712+472 and B1600+434, and $850\mu\text{m}$ dust upper limits are given for those sources in Table 2. Significant dust fluxes above the synchrotron power law were derived from the fits to MG J0414+0534, B1608+656, and B1938+666. The corrected fluxes for these three objects are given in Table 2. We estimate that that the correction adds an additional uncertainty of about 20% to the $850\mu\text{m}$ fluxes of MG J0414+0534 and B1938+666, and about 30% for B1608+656. These are added in quadrature to the statistical give the uncertainties quoted in Table 2.

A small flux correction is required for F10214+4724, which was measured at $800\mu\text{m}$ (Rowan-Robinson et al. 1993) rather than $850\mu\text{m}$. The flux corrected to $850\mu\text{m}$, and listed in Table 2, is 42.7 mJy. The dust template adopted above, with dust temperature $T_{\text{dust}} = 40\text{K}$ and emissivity index $\eta = 1.5$, was used for the correction.

K-corrections for computing *rest frame* $850\mu\text{m}$ luminosities are also derived using this same dust template. This

is the template used by ADH01 (which see for rationale, discussion of potential errors introduced by assuming the wrong template parameters, and references). To facilitate comparison with the radio galaxy results their units of luminosity are also adopted, L_{850} ($\text{W Hz}^{-1} \text{sr}^{-1}$), as is their method of computing dust masses using

$$M_{dust} = \frac{S_{obs} D_L^2}{(1+z)\kappa_{\nu_r} B_{\nu_r}(T_{dust})}, \quad (2)$$

where S_{obs} is the observed flux density, D_L is the luminosity distance, κ_{ν_r} is the mass absorption coefficient of the dust at ν_r (assumed to be equal to $0.15 \text{ m}^2 \text{kg}^{-1}$ at $800 \mu\text{m}$, and scaled to other wavelengths using $\lambda^{-1.5}$), and $B_{\nu_r}(T_{dust})$ is the intensity of a blackbody at ν_r assuming isothermal emission from dust grains at temperature T_{dust} .

3. DISCUSSION

Of the 40 sources presented in Table 1, 23 have clear detections of dust emission (see Table 2). This detection rate of 58% is almost twice that of the large survey of high redshift radio galaxies of ADH01, which detected 14/46 radio galaxies (30%) while going deeper in flux RMS (typically to 1 mJy) than the present survey and also using 2.0σ as the detection level (2.5σ is used here). The difference in detection rate is probably due to the lensing boost, rather than significant differences between the dust luminosities of quasars and radio galaxies, as shown below. Another recent AGN survey, of $z \approx 4$ quasars by Omont et al. (2001), had a 29% detection rate in observations at 1.2mm that had an average depth approximately equivalent to ours at $850 \mu\text{m}$ (assuming a dust emissivity exponent η of 1.5).

3.1. Mean Luminosities

Establishing the mean $850 \mu\text{m}$ dust luminosity and dust mass for the lensed quasar sample, and investigating whether these quantities are a function of redshift, is complicated by the presence of upper limits (17 out of 40 measurements). Extracting statistical information from the data requires survival analysis techniques, and here we use the ASURV software package developed by T. Isobe, M. LaValley, and E. Feigelson. This package provides correlation analysis, estimates of mean values, and linear regression parameters for samples containing both detections and upper limits.

However, some caveats apply. Estimation of the mean for flux-limited samples using survival analysis is not very robust when the upper limits are found mostly at the low end of the distribution, tending to bias the estimation upward relative to the true value as the percentage of upper limits increases. Conversion of fluxes to luminosities usually scrambles the upper limits because sources are at varying distances, mitigating the bias effect when applied to luminosities. However, in this case the luminosities are nearly independent of distance because of the steep negative K correction, so the upper limits in luminosity, like those in flux, are also largely clustered near the bottom.

Here we analyze the lensed quasars in this sample, and compare with the radio galaxies of ADH01. For these two samples, the radio galaxies would be more biased than

the lensed quasars because of the higher fraction of upper limits. On the positive side, the upper limits and detections for both samples are mixed to some extent because of non-uniform flux limits and, for the lensed quasars, the application of different boost factors. We will proceed with survival analysis with the recognition that the results probably represent upper limits to the true mean luminosities.

That noted, the mean of a sample with upper limits can be computed using the Kaplan-Meier estimator provided in ASURV. Applying this to the quasar sample, for $\Omega_0 = (1.0, 0.1)$, gives $\langle \log(L_{850}) \rangle = (22.47, 22.87) \text{ WHz}^{-1} \text{sr}^{-1}$, for 23 detections and 17 upper limits. Using the data of ADH01 to calculate the mean luminosity for radio galaxies, $\langle \log(L_{850}) \rangle = (22.82, 23.19) \text{ WHz}^{-1} \text{sr}^{-1}$, for 14 detections and 32 upper limits. At face value it would appear that radio galaxies are more luminous than quasars in the submillimeter by a factor of 2 or so, but the bias caused by the larger number of upper limits in the radio galaxy sample could easily account for such a difference. The bias would be particularly severe if the luminosity function is steep and has many more weak sources than strong ones, as is almost certainly the case (see the $850 \mu\text{m}$ luminosity function of local IRAS galaxies in Dunne et al. 2000). A precise comparison between the samples is further complicated by uncertainties in the lensing magnifications of the quasars. We conclude that the dust luminosities of high-redshift quasars and radio galaxies are qualitatively similar.

How do the high redshift quasars compare with local objects? From Table 2, the *detected* quasars have dust luminosities in the range $21.66 < \log(L_{850}) < 23.14 \text{ WHz}^{-1} \text{sr}^{-1}$ for $\Omega_0 = 1.0$ (for $\Omega_0 = 0.1$, the numbers are about twice as high). In the local universe, a number of quasars and Seyfert 1 galaxies have been observed at $850 \mu\text{m}$, and the luminosities of the detected ones typically fall within the range of the detected members of the high- z sample. For example, the luminosities of I Zw 1 (0050+124; $z = 0.061$), Mrk 1014 (0157+001; $z = 0.163$), and Mrk 376 (0710+457; $z = 0.056$) are: $\log(L_{850}) = 22.18, 22.94, \text{ and } 22.06$ respectively (using fluxes from Hughes et al. 1993).

A comparison can also be made with local (non-radio) galaxies. Results are available from a SCUBA survey of a large sample of nearby galaxies ($z < 0.07$) selected from the IRAS Bright Galaxy Sample. Measurements of 104 galaxies with $S_{60} > 5.24 \text{ Jy}$ are reported by Dunne et al. (2000); all were detected at $850 \mu\text{m}$. Roughly 65% are bright enough (assuming $H_0 = 50 \text{ km s}^{-1} \text{Mpc}^{-1}$) to fall within the definition of Luminous Infrared Galaxies (LIRGs), i.e., galaxies with $L_{\text{IR}} = L(8 - 1000 \mu\text{m}) > 10^{11} M_{\odot}$.¹ A few would be classified as ULIRGs with $L_{\text{IR}} > 10^{12} M_{\odot}$, and the rest have total infrared luminosities below $10^{11} M_{\odot}$.

In terms of monochromatic $850 \mu\text{m}$ luminosities, the range for the nearby IRAS galaxies is $20.35 < \log(L_{850}) < 22.95 \text{ WHz}^{-1} \text{sr}^{-1}$, and the mean value is 22.15 .² On average therefore the quasars, with $\log(L_{850}) \sim 22.7 \text{ WHz}^{-1} \text{sr}^{-1}$ (taking a value intermediate between $\Omega_0 = 0.1$ and 1), are not too different from local infrared-bright

¹ Dunne et al. computed the far-infrared 40 – 1000 μm values, L_{FIR} , but given the steep mid-infrared galaxy spectra this approximates the 8 – 1000 μm luminosities within a few percent.

² These values are independent of Ω_0 because the galaxies are nearby.

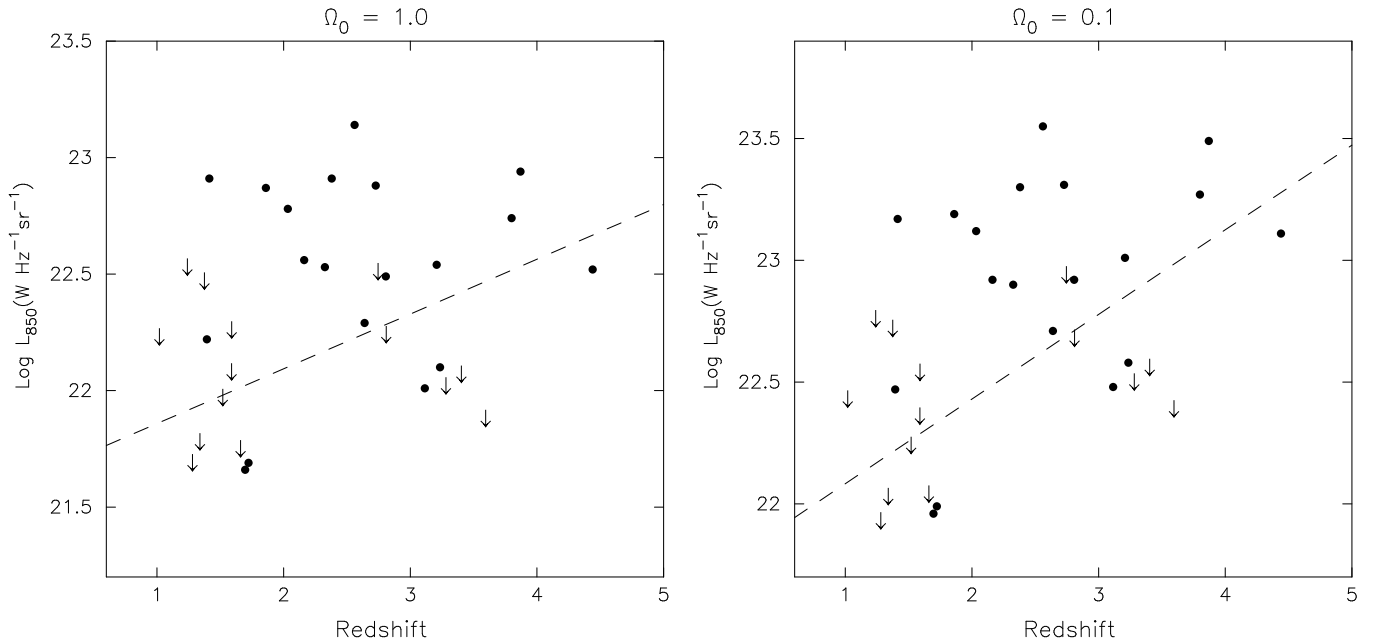


FIG. 2.— Monochromatic luminosity at $850\mu\text{m}$ versus redshift for the two cosmologies considered. The dashed lines represent best fit linear regressions, taking upper limits into account using the Buckley-James algorithm supplied in ASURV. A plot with $\Omega_M = 0.3$ and $\Omega_\Lambda = 0.7$ would appear intermediate between these two. Only sources with measured redshifts are plotted.

galaxies: their mean monochromatic $850\mu\text{m}$ luminosity is a few times higher.

To estimate the total infrared luminosities of the quasars, a template spectrum is needed to scale from L_{850} to $L_{IR}(8-1000\mu\text{m})$. The local quasar I Zw 1 has a well-measured infrared/submillimeter spectrum (see Hughes et al. 1993) and fits the bill – its spectrum is flat in νS_ν throughout the infrared and falls off sharply longward of $100\mu\text{m}$, typical of most quasars. This is in contrast to IRAS galaxies, which, because of a sharp dropoff from $60\mu\text{m}$ to $25\mu\text{m}$, have relatively little power in the mid-infrared. A I Zw 1–like spectrum was integrated to derive an approximate conversion factor from L_{850} to $L_{IR}(8-1000\mu\text{m})$ of $1.2 \times 10^{-10} L_\odot (\text{WHz}^{-1}\text{sr}^{-1})^{-1}$. Using this, the estimated mean 8 to $1000\mu\text{m}$ infrared luminosity of the quasars is $\langle L_{IR}(8-1000\mu\text{m}) \rangle \sim 6 \times 10^{12} h_{50}^{-2} L_\odot$, where h_{50} is the Hubble constant in units of $50 \text{ km s}^{-1} \text{ Mpc}^{-1}$. This means that the bolometric infrared luminosities of quasars are typically well into the range defined by ULIRGs. The mean total infrared luminosity of the local IRAS galaxies of Dunne et al. (2000) is $1.3 \times 10^{11} h_{50}^{-2} L_\odot$, about 45 times below that of the quasars. Thus, while the submillimeter luminosities of quasars are only a few times larger than IRAS galaxies, their total infrared luminosities are much larger. This is because quasars have much flatter mid-infrared spectra, and substantially more power there.

3.2. Relation Between Luminosity and Redshift

Figure 2 plots the quasar $850\mu\text{m}$ luminosities versus redshift for $\Omega_0 = 1.0$ and 0.1 , including only sources with measured redshifts. Ignoring the dashed regression lines for the moment, the eye picks up a slight trend of increasing luminosity with redshift for $\Omega_0 = 1$, and a definite trend for $\Omega_0 = 0.1$. Because of the strongly negative K correction, observed fluxes for a given submillimeter luminosity are essentially constant with redshift above $z = 1$

for $\Omega_0 = 1$, and slightly declining for $\Omega_0 = 0.1$ (see Figure 3).

Thus the usual situation where flux-limited samples tend to pick up higher luminosity objects at high redshift does not apply to submillimeter-selected samples, or only weakly. The samples presented here, and by ADH01, were not selected at submillimeter wavelengths however. ADH01 mitigated against potential selection effects at other wavelengths by selecting radio galaxies covering only a narrow range of radio luminosity. This approach was not possible for our sample of lensed quasars, though would naturally be adopted in any well-planned survey of field quasars. We must therefore consider the possibility that the observed trends with redshift are caused by sample anomalies. To this end, we have investigated possible correlations between optical/radio luminosity and redshift. No correlations are found, indicating that selection effects at other wavelengths are not responsible for the submillimeter trends.

The plotted regression lines take into account the upper limits, and are derived using the Buckley-James method in ASURV. They provide a stronger and more quantitative indication of a trend with redshift than the eye alone, since at first glance the upper limits tend to be interpreted as detections. But since more of the upper limits lie at low redshifts, they pull that end of the regression line down.

ASURV provides three test statistics for determining the probability that a correlation exists within a given data set: Cox’s Proportional Hazard Model, Generalized Kendall’s Tau, and Generalized Spearman’s Rho. ASURV actually computes the probability that no correlation is present (the null hypothesis); the results are listed in Table 3. For $\Omega_0 = 1$, the probability of *no correlation present* lies in the range 4 – 12%, depending on the test. The meaning of this for the Cox test, for example, is that in 96% of randomly distributed samples the degree of correlation

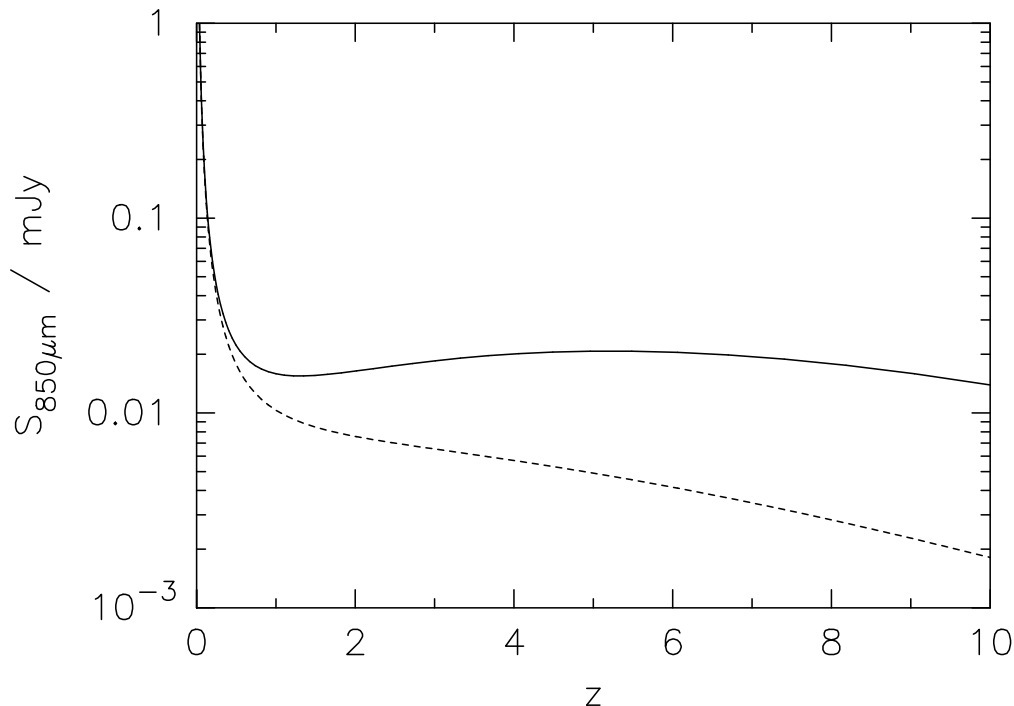


FIG. 3.— The observed $850\mu\text{m}$ flux density as a function of redshift for a submillimeter source having the dust emission template adopted in this paper, with $\eta = 1.5$ and $T_{dust} = 40\text{K}$. The solid line is for an $\Omega = 1.0$ universe, and the dashed line is for $\Omega = 0.1$. Figure courtesy of E.N. Archibald.

would be lower. For $\Omega_0 = 0.1$ the correlation is stronger, and the null probability lies in the range $0.8 - 2.5\%$.

Altering the dust template can change the degree of correlation and the slope of the luminosity–redshift relation. Lower temperatures and smaller values of η strengthen the relation, while higher temperatures and larger values of η weaken it. For the worst case we consider reasonable, with $\eta = 2$ and $T_{dust} = 60\text{K}$, the correlation breaks down for $\Omega = 1$, but remains reasonably significant for $\Omega = 0.1$. The correlation probabilities for this template are also shown in Table 3. However, evidence from other studies suggests that η is well under 2, and T_{dust} is in the range $35 - 50\text{K}$ (Benford et al. 1999; Dunne et al. 2000; Ivison et al. 2000).

The total uncertainties in the submillimeter luminosity estimates for this sample derive from the chosen cosmology, the applied magnification factor, the synchrotron correction (for three sources), the K-correction (dust template), and the statistical uncertainties in the flux measurements. Uncertainties in the synchrotron correction have been accounted for in the error estimates given in Table 2. The chosen Hubble Constant gives a constant offset, while the cosmological density parameter produces a redshift dependence. Computations with $\Omega = 0.1$ and 1.0 provide the extremes of this dependence. The K-correction also yields a redshift dependence, which has been addressed by taking a very unfavorable (and unlikely, we think) dust template and assessing the luminosity–redshift relation for that case.

Estimated uncertainties in luminosity for a given source (relative to others in the sample) are probably roughly a factor of 3 when all is taken into account. Some of the

uncertainty is random (e.g., magnification) and some is systematic. We believe we have covered the reasonable ranges of systematic error and conclude that the general trend of submillimeter luminosity increasing with redshift is likely to be real. However, given the uncertainties, the trend cannot be said to be proven by the data.

Considering the redshift dependence of radio galaxies, the null probabilities for no correlation between L_{850} and z listed by ADH01 are $0.0 - 0.2\%$ for $\Omega_0 = 1$, and 0.00% (all three statistics) for $\Omega_0 = 0.1$; clearly the statistical evidence, from survival analysis, of increasing luminosity with redshift is stronger for the radio galaxies. This does not mean that the *rate* of increase is stronger, but rather that the scatter in the distribution is somewhat lower for the radio galaxies than for the quasars in these samples. For the $\Omega_0 = 0.1$ case, both distributions show roughly an order of magnitude increase from $z = 1$ to $z = 4$. Most of the increased probability of correlation for the radio galaxies appears to be based on three quite luminous objects at $z \sim 4$ (see Figure 4 of ADH01). We hypothesize that the larger scatter in the quasar distribution is caused by two effects: the larger number of detections, providing a broader probe of the luminosity function, and uncertainties in the lensing corrections.

3.3. Comparing Radio Loud and Radio Quiet Quasars

Do radio loud and radio quiet quasars have different submillimeter properties? The Kaplan-Meier estimator has been applied to the radio loud and quiet luminosities separately, resulting in (for $\Omega = 1$) $\langle L_{850}(\text{RLQ}) \rangle = 2.3 \pm 0.7 \times 10^{22} \text{ WHz}^{-1} \text{sr}^{-1}$ and $\langle L_{850}(\text{RQQ}) \rangle = 3.4 \pm 0.7 \times 10^{22}$

$\text{WHz}^{-1}\text{sr}^{-1}$, with 9 detections and 8 upper limits for the RLQs and 14 detections and 9 upper limits for the RQQs. These values are consistent with each other to within the errors, and we conclude that there is no evidence here for a systematic difference in submillimeter luminosity between radio loud and quiet quasars. This similarity in dust properties between optical and radio selected quasars suggests that there is no dust-related difference between radio loud and radio quiet AGN, as might be expected if one population resided in more massive systems than the other.

Comparison between the quasar types for correlations with redshift was not possible because of the small number of detected radio loud quasars having measured redshifts (5 detections out of 11 objects).

4. SUMMARY AND CONCLUSIONS

The present submillimeter survey of lensed quasars shows that the dust luminosities/masses of quasars are comparable to those of radio galaxies (Archibald et al. 2001) in the same redshift range ($1 \lesssim z \lesssim 4.4$), and that quasars, like radio galaxies, appear to have increasingly powerful dust sources toward higher redshifts. The mean monochromatic $850\mu\text{m}$ luminosity of high-redshift quasars is only a few times higher than that of a local sample of IRAS-selected galaxies, but because quasars have more power in the mid-infrared their total infrared luminosities ($8 - 1000\mu\text{m}$) are substantially greater.

The concordance of mean dust luminosity and luminosity evolution with redshift between quasars and radio galaxies is broadly consistent with, and supportive of, obscuration/orientation unified schemes wherein these classes are by and large similar except for chance viewing angle. The submillimeter dust flux is likely to be optically thin and therefore orientation independent. The presence or absence of a strong radio source appears to have little effect on the submillimeter power once synchrotron contamination has been accounted for, and this argues against large differences in the total masses of radio quiet versus radio loud systems.

The tentative evidence presented here for higher dust luminosities and inferred dust masses at high redshift could have several interpretations. One possibility is that the increase is illusory, for example if dust properties change over cosmic time in such a way as to cause an increased emissivity per unit dust mass at high z , or if the spectral energy distribution of grain emission changes with time causing the *derived* relative luminosities/masses to change. The template SED used here is not necessarily the correct one in general, and cannot be correct for all specific objects since galaxy studies have shown a fair amount of variation in the far-IR/submillimeter SEDs from one object to the next (see, e.g., Figure 2 of Adelberger & Steidel 2000). Other SED shapes can dampen the trend with redshift (while yet others can strengthen it). Greenberg & Shen (2000) have stressed that dust in the early universe could be much different than it is today, but the form of any

cosmic evolution of mean dust properties from $z = 4$ to $z = 1$ is anybody's guess.

Dust sources in quasars are powered by absorption of energy from the central AGN and by star formation, with the proportionate mix between the two being in general unknown. An increased mass of dust in early galaxies could come about because of more frequent galaxy interactions and mergers when the universe was smaller and more dense. These mergers could, in addition to dumping mass into the central regions of the host galaxy, trigger vigorous star formation to power the dust.

Alternatively, if the primary energy source for the grains is the central AGN, the increased luminosity could be caused by a larger dust covering factor at higher z , meaning that more of the quasar light would be intercepted and reprocessed into IR/submillimeter emission. A larger covering factor could result from a larger total dust mass, or simply a larger fraction of the dust being exposed to the primary radiation. If there is a torus surrounding the AGN, it could be physically thicker (i.e., smaller opening angle). A second possibility is that material has not had a chance to settle into an optically thick torus because of the youth of the systems and their more violent environments, leaving relatively more of the grains exposed to the nuclear radiation. The larger covering factor interpretation implies a larger fraction of obscured AGNs at high redshifts, as a lower proportion of direct quasar light escapes to distant observers.

Models for the x-ray background are still uncertain, but recent work by Gilli et al. (2001) finds a better fit to the currently available x-ray data with an increasing ratio of obscured to unobscured AGNs toward higher redshifts. That particular model seems to indicate that the evolution stops above about $z = 1.5$. The increasing dust luminosity with redshift found by Archibald et al. (2001) for radio galaxies, and the similar relation found here for quasars, suggests that the proportion of obscured AGNs may continue to increase out to $z = 2$ or beyond.

The authors thank the JCMT for generous allocations of telescope time for this project, and Iain Coulson for help with some of the observations. Frank Bertoldi kindly obtained some of the IRAM 1.3mm bolometer data. We thank Joseph Lehar and Brian McLeod for providing lensing magnifications from the Castles project, and Ski Antonucci and Andrew Blain for comments on the manuscript. Brian McLeod contributed substantially to our understanding of magnification effects by running magnification versus source size models for use in Figure 1. Eric Fiegelson kindly provided advice on the use of ASURV and interpretation of its output, and Else Archibald granted permission to use Figure 3. We are grateful to the referee for helpful suggestions. The CASTLeS web page, <http://cfa-www.harvard.edu/castles>, was used extensively, as was the NASA Extragalactic Database (NED).

REFERENCES

- Adelberger, K.L., & Steidel, C.C. 2000, *ApJ*, 544, 218
 Archibald, E.N., Dunlop, J.S.; Hughes, D.H.; Rawlings, S.; Eales, S.A.; Ivison, R.J. 2001, *MNRAS*, 323, 417 (ADH01)
 Barvainis, R., Alloin, D., & Bremer, M. 2002, *A&A*, in press
 Barvainis, R., Antonucci, R., & Coleman, P. 1992, *ApJ*, 399, L19
 Barvainis, R., Antonucci, R., Hurt, T., Coleman, P., & Reuter, H.-P. 1995, *ApJ*, 451, L9

- Benford, D.J., Cox, P., Omont, A., Phillips, T.G., & McMahon, R.G. 1999, *ApJ*, 518, L65
- Blain, A.W. 1999, *MNRAS*, 304, 669
- Downes, D., Solomon, P.M., & Radford, S.J.E. 1995, *ApJ*, 453, L65
- Downes, D., Neri, R., Wiklind, T., Wilner, D.J., & Shaver, P.A. 1999, *ApJ*, 513, L1
- Dunne, L., Eales, S., Edmunds, M, Ivison, R., Alexander, P., & Clements, D. 2000, *MNRAS*, 315, 115
- Eisenhardt, P. R., Armus, L., Hogg, D.W., Soifer, B. T., Neugebauer, G., Werner, M.W. 1996, *ApJ*, 461, 72
- Gilli, R., Salvati, M., & Hasinger, G. 2001, *A&A*, 366, 407
- Greenberg, J.M., & Shen, C. 2000, *astro-ph/0006337*
- Holland et al. 1999, *MNRAS*, 303, 659
- Hughes, D.H., Dunlop, J.S., & Rawlings, S. 1997, *MNRAS*, 289, 766
- Hughes, D.H., Robson, E.I., Dunlop, J.S., & Gear, W.K. 1993, *MNRAS* 263, 607
- Ivison, R.J., et al. 2000, *MNRAS*, 315, 209
- Jenness & Lightfoot 1998
- Kneib, J.-P., Alloin, D., Mellier, Y., Guilloteau, S., Barvainis, R., & Antonucci, R. 1998, *A&A*, 329, 827
- Kormendy, J., & Sanders, D.B. 1992, *ApJ*, 390, L53
- Lewis, G.F., Chapman, S.C., Ibata, R.A., Irwin, M.J., & Totten, E.J. 1998, *ApJ*, 505, L1
- Omont, A., Cox, P., Bertoldi, F., McMahon, R.G., Carilli, C., Isaak, K.G. 2001, *A&A*, 374, 371
- Planesas, P., Martin-Pintado, J., Neri, R., & Colina, L. 1999, *Science*, 286, 2493
- Rowan-Robinson, M., et al. 1991, *Nature*, 351, 719
- Rowan-Robinson, M., et al. 1991, *MNRAS*, 262, 513
- Sanders, D., & Mirabel, I.F. 1996, *ARA&A*, 34, 749
- Smail, I., Ivison, R.J., & Blain, A.W. 1997, *ApJ*, 490, L5
- Steidel, C.C., Adelberger, K.L., Giavalisco, M., Dickinson, M., & Pettini, M. 1999, *ApJ*, 519, 1
- Stevens, J.A., Ivison, R.J., Jenness, T. 1997, *Starlink Cookbook* 10.1
- van Dokkum, P.G., Franx, M., Favricant, D., Kelson, D.D., & Illingworth, G.D. 1999, *ApJ*, 520, L95

TABLE 1
MM/SUB-MM MEASUREMENTS OF LENSED QUASARS

Source	Type	z	S_{3000} (mJy)	S_{1300} (mJy)	S_{850} (mJy)	S_{450} (mJy)	Notes
0047–2808	RQQ	3.595	< 2.0	...	< 7.0	...	1
CLASS B0128+437	RLQ	—	< 6.0	...	
UM673	RQQ	2.727	< 1.3	< 5.8	12.0 (2.2)	< 40	
HE 0230–2130	RQQ	2.162	21.0 (1.7)	77 (13)	
MG J0414+0534	RLQ	2.639	40 (2.0)	20.7 (1.3)	25.3 (1.8)	66 (16)	2
CLASS B0712+472	RLQ	1.339	22 (0.4)	9.8 (1.4)	7.4 (1.8)	...	8,10
CLASS B0739+367	RLQ	—	...	< 2.8	6.6 (1.3)	36 (10)	2
MG J0751+2716	RLQ	3.208	4.1 (0.5)	6.7 (1.3)	25.8 (1.3)	71 (15)	1
HS 0818+1227	RQQ	3.115	4.6 (1.7)	< 83	
APM 08279+5255	RQQ	3.870	...	24 (2)	84 (3)	285 (11)	3
SBS 0909+532	RQQ	1.375	< 0.8	< 2.3	< 5.5	...	2
RX J0911.4+0551	RQQ	2.807	1.7 (0.3)	10.2 (1.8)	26.7 (1.4)	65 (19)	1
RX J0921+4529	RQQ	1.66	< 4.3	...	
FBQS J0951+2635	RQQ	1.24	...	< 2.5	< 3.8	...	2
BRI 0952–0115	RQQ	4.440	...	< 2.3	13.4 (2.3)	...	2,4
0957+561	RLQ	1.413	14.2	< 4.0	7.5 (1.4)	...	5
LBQS 1009–0252	RQQ	2.746	...	< 5.0	< 4.5	< 58	2
IRAS F10214+4724	RQQ	2.380	...	24 (5)	50 (5)	273 (45)	6
HE 1104–1805	RQQ	2.326	< 5.0	5.3 (0.9)	14.8 (3.0)	...	2
PG 1115+080	RQQ	1.723	< 0.8	< 3.0	3.7 (1.3)	...	1
CLASS B1127+385	RLQ	—	...	< 2.8	13.9 (2.3)	< 65	2
CLASS B1152+199	RLQ	1.019	< 6.5	< 70	
1208+1011	RQQ	3.8	< 0.9	2.8 (0.9)	8.1 (2.0)	...	2
HST 12531–2914	RQQ	—	< 6.4	...	
CLASS B1359+154	RLQ	3.235	11.5 (1.9)	39 (10)	
HST 14113+5211	RQQ	2.81	< 3.6	...	
H 1413+117	RQQ	2.560	...	18.0 (2.0)	58.8(8.1)	224 (38)	2,7
HST 14176+5226	RQQ	3.403	< 0.9	< 4.0	< 3.5	< 26	2
SBS 1520+530	RQQ	1.860	< 0.6	2.8 (0.8)	9.4 (2.6)	...	2
CLASS B1555+375	RLQ	1.59	< 6.8	< 39	
CLASS B1600+434	RLQ	1.589	25 (0.3)	12.6 (2.3)	7.3 (1.8)	...	1,10
CLASS B1608+656	RLQ	1.394	8.1 (0.4)	5.6 (1.7)	8.1 (1.7)	...	9
FBQS J1633+3134	RQQ	1.520	< 3.5	...	
CLASS B1938+666	RLQ	—	...	14.7 (2.0)	34.6 (2.0)	126 (22)	9
MG J2016+112	RLQ	3.282	1.8 (0.2)	< 2.5	< 4.8	...	1
CLASS B2045+265	RLQ	1.280	< 3.7	< 22	
CLASS B2114+022	RLQ	—	< 4.3	...	
HE 2149–2745	RQQ	2.033	< 6.8	...	8.0 (1.9)	...	1
2237+0305	RQQ	1.696	< 0.8	...	2.8 (0.9)	< 17	1
CLASS B2319+051	RLQ	—	...	< 3	3.9 (1.2)	40 (8)	2

Notes. — (1) IRAM PdBI observations at both 3mm and 1mm (where reported). (2) IRAM PdBI at 3mm (where reported), IRAM 30m telescope at 1.3mm. (3) Also detected by Lewis et al. (1998) at 850 and 450 μ m, our measurements reported here; 1.3mm flux from Lewis et al. (1998). (4) Also detected at 850 μ m by McMahon et al. (1999). (5) 3mm flux from Planesas et al. (1999). 1.3mm flux from IRAM 30m. (6) All fluxes from Rowan-Robinson et al. (1993); measurements at 1100 μ m, 800 μ m, and 450 μ m. (7) 450 μ m flux from Barvainis et al. (1992, 1995); 850 μ m flux from this work. (8) 1.3mm measurement is weighted average of fluxes from IRAM PdBI and 30m telescope. 3mm flux is from PdBI. (9) 1.3mm flux from JCMT using SCUBA. 3mm flux from PdBI (where reported). (10) Consistent with pure synchrotron.

TABLE 2
850 μ m LUMINOSITIES AND DUST MASSES

Source	z^a	S_{850}^b (mJy)	m^c (model)	m^d (adopted)	$\Omega_0 = 1.0, H_0 = 50$		$\Omega_0 = 0.1, H_0 = 50$		Refs ^e
					$\log L_{850}$ (WHz ⁻¹ sr ⁻¹)	$\log M_{dust}$ (M_\odot)	$\log L_{850}$ (WHz ⁻¹ sr ⁻¹)	$\log M_{dust}$ (M_\odot)	
0047–2808	3.595	< 7.0	22.4	20.0	< 21.88	< 7.35	< 22.39	< 7.86	1
CLASS B0128+437	<i>2.400</i>	< 6.0	...	10.0	< 22.15	< 7.63	< 22.55	< 8.02	
UM673	2.727	12.0(2.2)	3.7	3.7	22.88	8.35	23.31	8.77	1
HE 0230–2130	2.162	21.0 (1.7)	14.5	14.5	22.56	8.03	22.92	8.39	1
MG J0414+0534	2.639	16.7 (3.8)	26.9	20.0	22.29	7.76	22.72	8.18	1
CLASS B0712+472	1.339	< 4.5	50.1	20.0	< 21.78	< 7.25	< 22.03	< 7.50	1
CLASS B0739+667	<i>2.400</i>	6.6 (1.3)	...	10.0	22.20	7.67	22.59	8.06	
MG J0751+2716	3.208	25.8 (1.3)	16.6	16.6	22.54	8.01	23.01	8.48	1
HS 0818+1227	3.115	4.6 (1.7)	...	10.0	22.01	7.48	22.48	7.95	
APM 08279+5255	3.870	84.0 (3.0)	100	20.0	22.94	8.42	23.49	8.96	2
SBS 0909+532	1.375	< 5.5	5.0	5.0	< 22.47	< 7.94	< 22.72	< 8.19	1
RX J0911.4+0551	2.807	26.7 (1.4)	21.8	20.0	22.49	7.96	22.92	8.39	1
RX J0921+4528	1.660	< 4.3	23.2	20.0	< 21.75	< 7.22	< 22.04	< 7.51	1
FBQS J0951+2635	1.240	< 3.8	3.0	3.0	< 22.53	< 8.00	< 22.76	< 8.22	1
BRI 0952–0115	4.440	13.4 (2.3)	8.3	8.3	22.52	7.99	23.11	8.57	1
0957+561	1.413	7.5 (1.4)	2.5	2.5	22.91	8.39	23.17	8.64	1
LBQS 1009–0252	2.746	< 4.5	3.2	3.2	< 22.51	< 7.98	< 22.94	< 8.40	1
IRAS F10214+4724	2.380	42.7 (5.0)	100	13.0	22.91	8.38	23.30	8.76	3
HE 1104–1805	2.326	14.8 (3.0)	10.8	10.8	22.53	8.00	22.90	8.37	1
PG 1115+080	1.723	3.7 (1.3)	27.7	20.0	21.69	7.16	21.99	7.46	1
CLASS B1127+385	<i>2.400</i>	13.9 (2.3)	3.0	3.0	23.05	8.52	23.44	8.91	1
CLASS B1152+199	1.019	< 6.5	...	10.0	< 22.23	< 7.71	< 22.43	< 7.90	
1208+1011	3.800	8.1 (2.0)	3.1	3.1	22.74	8.21	23.27	8.74	1
HST 12531–2914	<i>2.400</i>	< 6.4	7.8	7.8	< 22.29	< 7.77	< 22.68	< 8.15	1
CLASS B1359+154	3.235	11.5 (1.9)	118	20.0	22.10	7.57	22.58	8.05	1
HST 14113+5211	2.810	< 3.6	4.8	4.8	< 22.24	< 7.71	< 22.68	< 8.14	1
H 1413+117	2.560	58.8 (8.1)	9.6	9.6	23.14	8.61	23.55	9.02	1
HST 14176+5226	3.403	< 3.5	6.6	6.6	< 22.07	< 7.54	< 22.56	< 8.03	1
SBS 1520+530	1.860	9.4 (2.6)	3.3	3.3	22.87	8.34	23.19	8.66	1
CLASS B1555+375	1.59	< 6.8	...	10.0	< 22.22	< 7.69	< 22.61	< 8.07	
CLASS B1600+434	1.589	< 4.5	...	10.0	< 22.08	< 7.55	< 22.36	< 7.83	
CLASS B1608+656	1.394	6.6 (2.6)	10.8	10.8	22.22	7.69	22.47	7.94	1
FBQS J1633+3134	1.520	< 3.5	...	10.0	< 21.97	< 7.44	< 22.24	< 7.71	
CLASS B1938+666	<i>2.400</i>	32.0 (6.7)	173	20.0	22.59	8.06	22.98	8.44	1
MG J2016+112	3.282	< 4.8	...	10.0	< 22.02	< 7.49	< 22.50	< 7.97	
CLASS B2045+265	1.280	< 3.7	81.2	20.0	< 21.69	< 7.16	< 21.93	< 7.40	1
CLASS B2114+022	<i>2.400</i>	< 4.3	...	10.0	< 22.01	< 7.48	< 22.40	< 7.87	
HE 2149–2745	2.033	8.0 (1.9)	3.4	3.4	22.78	8.25	23.12	8.59	1
2237+0305	1.696	2.8 (0.9)	16.0	16.0	21.66	7.14	21.96	7.43	1
CLASS B2319+051	<i>2.400</i>	3.9 (1.2)	...	10.0	21.98	7.45	22.36	7.83	

^aRedshifts in italics are assumed, based on mean of the known redshifts for this sample.

^b850 μ m fluxes corrected in 3 cases (MG J0414+0534, B1608+656, and B1938+666) for synchrotron contamination, or a small difference in wavelength from 850 μ m (F10214+4724). Quoted uncertainties have been increased to account for the uncertainties in the synchrotron corrections; see Section 2.4 of the text.

^cLensing magnification based on models of the optical or centimeter radio emission. See footnote (e) for references.

^dAdopted magnifications: if there is no model available, m is set to 10.0; if the model gives $m > 20$, $m = 20.0$ is assumed (with the exception of F10214+4724; see footnote (e)). See §2.2 for discussion.

^eReferences for the magnifications are (1) J. Lehar & B. McLeod (2001, private communication); (2) Egami et al. (2000); (3) optical value from Eisenhardt et al. (1996), adopted value based on submillimeter estimate from Downes et al. (1995).

TABLE 3
 L_{850} VS. REDSHIFT CORRELATION RESULTS

ASURV Test	Probability of No Correlation Present			
	<i>Nominal case</i>		<i>Worst case</i>	
	$\beta = 1.5, T = 40K$		$\beta = 2.0, T = 60K$	
	$\Omega_0 = 1.0$	$\Omega_0 = 0.1$	$\Omega_0 = 1.0$	$\Omega_0 = 0.1$
Cox Proportional	4.1%	0.8%	20%	4.1%
Kendall's Tau	11.9%	2.5%	39%	10%
Spearman's Rho	6.9%	1.3%	26%	6.5%